IEEE Photonics Journal
An IEEE Photonics Society Publication

Open Access

# Resonant Wavelength Shift Detection System Based on a Gradient Grating Period Guided-Mode Resonance

Volume 10, Number 4, August 2018

Chih-Wei Chang
Shi-Ting Chen
Yi-Ming Lin
Cheng-Sheng Huang

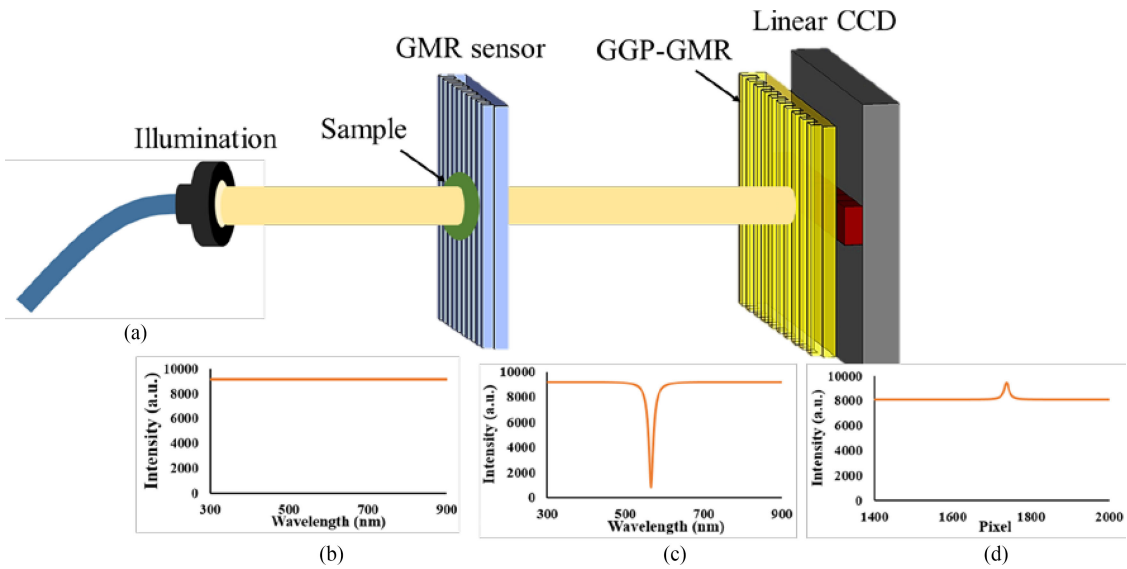


DOI: 10.1109/JPHOT.2018.2857505
1943-0655 © 2018 IEEE

# Resonant Wavelength Shift Detection System Based on a Gradient Grating Period Guided-Mode Resonance

**Chih-Wei Chang, Shi-Ting Chen, Yi-Ming Lin, and Cheng-Sheng Huang**

Department of Mechanical Engineering, National Chiao Tung University, Hsinchu 30010, Taiwan

*DOI:10.1109/JPHOT.2018.2857505*


Manuscript received June 4, 2018; revised July 9, 2018; accepted July 16, 2018. Date of publication July 19, 2018; date of current version July 31, 2018. This work was supported by the Ministry of Science and Technology (MOST) in Taiwan under Grants 106-3114-E-009-004 and 106-2221-E-009-120. Corresponding author: Cheng-Sheng Huang (e-mail: csh@nctu.edu.tw).
This paper has supplementary downloadable material available at http://ieeexplore.ieee.org.

**Abstract:** A resonant wavelength detection system based on a gradient grating period guided-mode resonance (GGP-GMR) filter and a linear charge-coupled device is demonstrated. The GGP-GMR used in this work consists of a subwavelength grating structure with a grating period that varies from 250 to 550 nm in increments of 2 nm. We successfully demonstrate that by using this system, we can monitor the shift in a sensor's dip wavelength caused by different sucrose concentrations. This technology has the potential to replace the spectrometer used in most optical biosensor systems. Given its compactness, the system can be integrated with lab-on-a-chip systems for numerous biosensing applications.

**Index Terms:** Gratings, optical filters, spectroscopy, subwavelength structures, wavelength measurement.

## 1. Introduction

Being able to quantify an unknown sample without using fluorescence labels is one of the greatest advantages of label-free (LF) biosensors. Among the numerous transducing mechanisms, LF biosensors based on optical transduction are the most widely used because of their high sensitivity, lack of electromagnetic interference, remote sensing capability, multiplexing, real-time monitoring, and compact design. Adsorbed biomolecules can trigger changes in various measurands. Various instruments have measured different measurands such as intensity, wavelength, and coupling angle caused by the change of refractive index (RI); different approaches and apparatus have been demonstrated successfully [1]. Among these approaches, monitoring the shift of wavelength is the most commonly used such as surface plasmon resonance [2], guided-mode resonance (GMR) filters [3], [4], photonic crystals (PCs) [5], and Bragg gratings [6], [7]. Depending on the designs and the intrinsic mechanisms of the optical sensors, the transmission or reflection spectra can be dip [2], [7], [8] or peak types [3]–[6], [9].

Although various palmtop spectrometers with acceptable resolution are available, they are too large to be integrated with lab-on-a-chip systems. To overcome this drawback, numerous researchers have been working on microspectrometers based on different mechanisms, including Fabry-Perot [10], gradient GMR filters [11], [12], PCs [13], and colloidal quantum dots [14]. De-

spite the potential of these microspectrometers, those that are available are highly complicated in fabrication [10], and others are still under development [11], [12]. Furthermore, sophisticated algorithms are often needed to reconstruct the spectra measured by such devices [11], [12], [14].

In this work, we propose a dip wavelength detection system based on a gradient grating period (GGP)-GMR filter and a linear charge-coupled device (CCD). The system can identify the dip wavelength from a GMR biosensor by translating the spectral information into spatial information in the CCD. When a broadband light source illuminates a GMR biosensor, a specific wavelength resonating with the GMR is reflected, resulting in a transmission spectrum with a dip wavelength (corresponding to the resonant wavelength). When such a transmission spectrum is incident on the GGP-GMR and CCD system, a transmission peak can be obtained from the resulting intensity distribution at the CCD. Based on a precalibrated transmission efficiency matrix, the pixel corresponding to the transmission peak correlates well with the dip wavelength.

To demonstrate the proposed idea, a GMR sensor was exposed to different concentrations of sucrose and illuminated with a broadband light source. The system generated a transmission spectrum with a dip wavelength corresponding to the device's resonance. When the concentrations of sucrose on the GMR sensor changed, the dip wavelength shifted in response to the change of refractive index (RI) resulting from the various concentrations of sucrose. Our system successfully translated the spectral shifts into spatial shifts in its CCD.

## 2. Method

### *2.1 Fabrication and Characterization of GGP-GMR*

At the core of our dip wavelength detection system is the GMR filter [15], which is also known as a PC [16]. The device is essentially a three-layer structure: substrate, waveguide, and cover layer. The GMR allows external light to be coupled into waveguide modes through phase matching provided by a subwavelength grating structure. The grating can be fabricated on the waveguide layer; it can be embedded between the substrate and the waveguide layer; it can also have other configurations as long as the grating structure overlaps with the guided modes. With proper design of the dimensions of the GMR, including the grating period, duty cycle, and depth, substrate, waveguide layer thickness, and device RIs, the resonance can be adjusted or optimized for particular applications.

Upon illumination at normal incidence, a specific wavelength of light is reflected back, and the rest of the light is transmitted through. This can be observed experimentally as a narrow-band reflection or a transmission dip. The wavelength of the reflection peak or the transmission dip is the resonant wavelength, which can be calculated from the second-order Bragg condition [17]:

$$\lambda = n_{eff}\Lambda \tag{1}$$

where $\lambda$ is the resonant wavelength, $n_{eff}$ is the effective index, and $\Lambda$ is the grating period. If the grating periods are gradually varied, the resonant wavelengths vary continuously across the device, which functions as a linear variable filter; this type of device is termed a GGP-GMR [18]. Gradient GMR based on graded waveguide thickness have also been purposed for other applications [19], [20]. The GGP-GMR used in this work was fabricated using replica molding and film deposition. The design and fabrication of the GGP-GMR were very similar to those reported previously [18]. In brief, a grating structure with gradient periods was fabricated using electron beam lithography on a silicon wafer. The grating period was varied from 250 to 550 nm in increments of 2 nm. In this work, each period consisted of 100 cycles; thus, the total length of the GMR was only approximately 6 mm. The grating depth was approximately 90 nm. A UV-curable polymer (NOA68, $n = 1.556$) was sandwiched between a Si master and a flexible sheet of polyethylene terephthalate (PET). An ultraviolet (UV) light (RC-742, Xenon) was used to illuminate and then cured the NOA68 before the NOA68/PET was separated from the Si master. Lastly, a layer of $TiO_2$ was sputter coated to complete the GGP-GMR. Fig. 1 shows a picture of the fabricated GGP-GMR on a PET sheet and scanning electron microscope images of top and cross-sectional views at different periods.

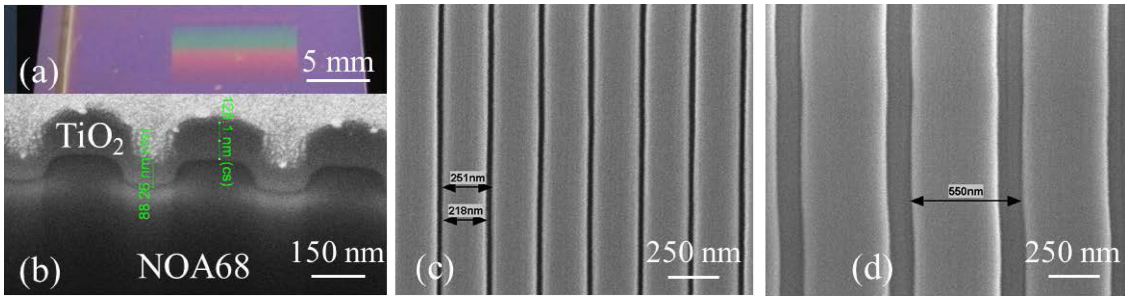


Fig. 1. (a) Photograph of a fabricated GGP-GMR on a PET sheet. The grating periods vary vertically. (b) Cross-sectional view of the GGP-GMR with a period of 376 nm. (c) Top view of the GGP-GMR with the smallest (250 nm) and largest (550 nm) period.

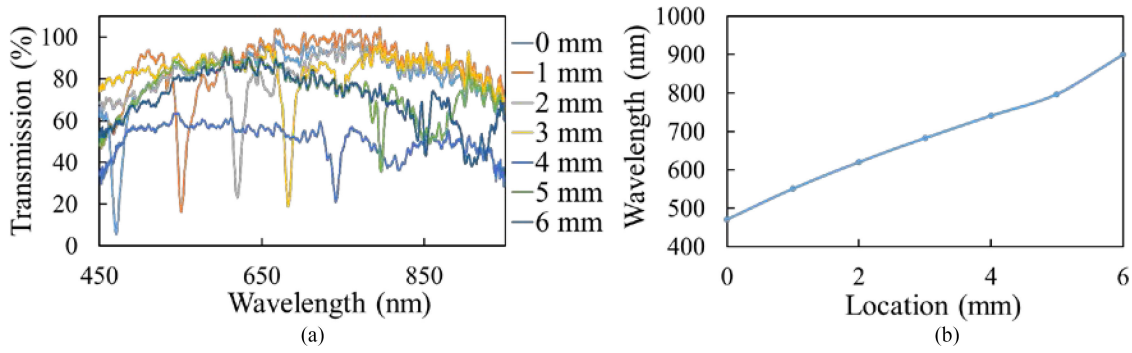


Fig. 2. (a) Transmission spectrum at seven different locations with different periods. (b) Relationship between the resonant wavelength and spatial locations.

Fig. 2(a) shows the transmission spectra for transverse magnetic (TM) polarization at different locations of the GGP-GMR filter. The resonant wavelength exhibits a fairly linear relationship with lateral distance, as shown in Fig. 2(b). At locations between 0 and 3 mm (corresponding to resonant wavelengths of 470.8 to 682.7 nm), the GGP-GMR exhibits effective coupling with approximately 20% transmission efficiency. The full width half maximum (FWHM) values are approximately 6–21 nm. At locations beyond 3 mm (corresponding to a relatively longer grating period), the coupling efficiency is noticeably degraded. A detailed discussion on GGP-GMR characterization and potential improvement was published previously [18]. For the purposes of this work, only the resonant range between 550–660 nm (less than 1.8 mm long based on Fig. 2) was used to detect the dip wavelength from a sensor; thus, the low coupling efficiency in the longer wavelength region is not of concern here.

### *2.2 Resonant Pixel Calibration*

The key concept of detecting the dip wavelength with the GGP-GMR and CCD system is to convert the spectral information of the incident light into spatial information at the CCD. To do so, the GGP-GMR was attached to a linear CCD (Toshiba TCD 1304), which has pixel size of 8 $\times$ 200 $\mu$m with total of 3648 pixels and a detection range between 330 and 1000 nm. A monochromator (DK242, Spectral Products) incorporated with a broadband light source (LSH-150, Taiwan Fiber Optics, Inc.) was used to generate a specific wavelength of light to obtain the resonant pixel at the CCD for the corresponding wavelength. The monochromator was set to illuminate a wavelength with a FWHM of 2.4 nm and a slit size of 1.5 mm. The monochromator illumination was TM-polarized and expanded to cover the entirety of the GGP-GMR. When a specific wavelength of light was incident on the GGP-GMR, it excited resonance at a specific location of the GGP-GMR, such that the light was reflected back at that location and was transmitted through at other locations. Hence, the

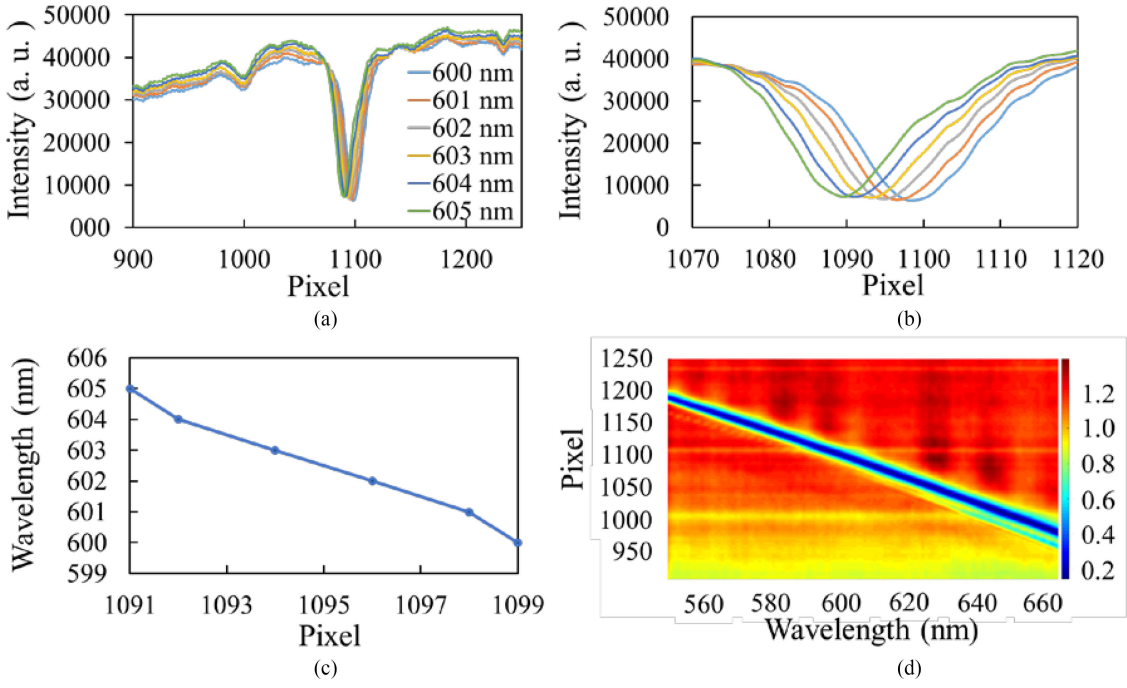


Fig. 3. (a) Intensity distribution on the CCD with incident wavelength of 600–605 nm. (b) Close-up at the resonant dip region. (b) Relationship between the resonant wavelength and resonant pixel. (c) Transmission efficiency at each resonant pixel for each wavelength.

pixel underneath that location measured a minimal intensity. Fig. 3(a) and 3(b) shows the intensity measured by the CCD for incident wavelengths of 600–605 nm. Clearly, as shown in the Fig. 3(b), for each wavelength a corresponding pixel (resonant pixel) results in minimal intensity. Fig. 3(c) shows the correlation between incident wavelength and resonant pixel; the designed GGP-GMR was able to distinguish a 1-nm difference clearly. Later passages discuss further improvements to resolution. The transmission efficiency for each resonant pixel at each wavelength can be calculated by dividing the intensity measured by the CCD with a GGP-GMR to that measured without a GGP-GMR. Fig. 3(d) shows the relationship between a specific wavelength and a resonant pixel with corresponding transmission efficiency, which was collected by sweeping the monochromator from 550–660 nm with a 1-nm increment. Over that wavelength range, the transmission efficiency was approximately 20%.

From Fig. 3(d), we can construct a transmission efficiency matrix, T. In this study, T is a square matrix with j $\times$ j elements; here, the first subscript indicates the resonant pixel, and the second subscript refers to a specific wavelength used for calibration. Essentially, each element in T represents transmission efficiency for a specific wavelength at a specific resonant pixel. For any incident spectrum, the light can be discretized to $I_j$ where the subscript corresponds to the specific wavelength used in calibration, such that the resulting intensity on the CCD can be calculated by $C = TI$ where C represents the discrete intensity at each resonant pixel.

### *2.3 Experimental Setup and Detection Method*

The key innovation of this work is to replace a spectrometer with a simple and compact GGP-GMR and CCD system to monitor the shift of the dip wavelength resulting from a response from a biosensor. In this work, a GMR sensor and the transmission modality were used to generate a dip wavelength response. Fig. 4(a) illustrates the experimental setup for detecting a dip wavelength and Fig. 4(b)–(d) represent the spectra at different stages through the optical path. When a broadband light source (Fig. 4(b)) illuminated at a GMR sensor with or without sample, a specific wavelength

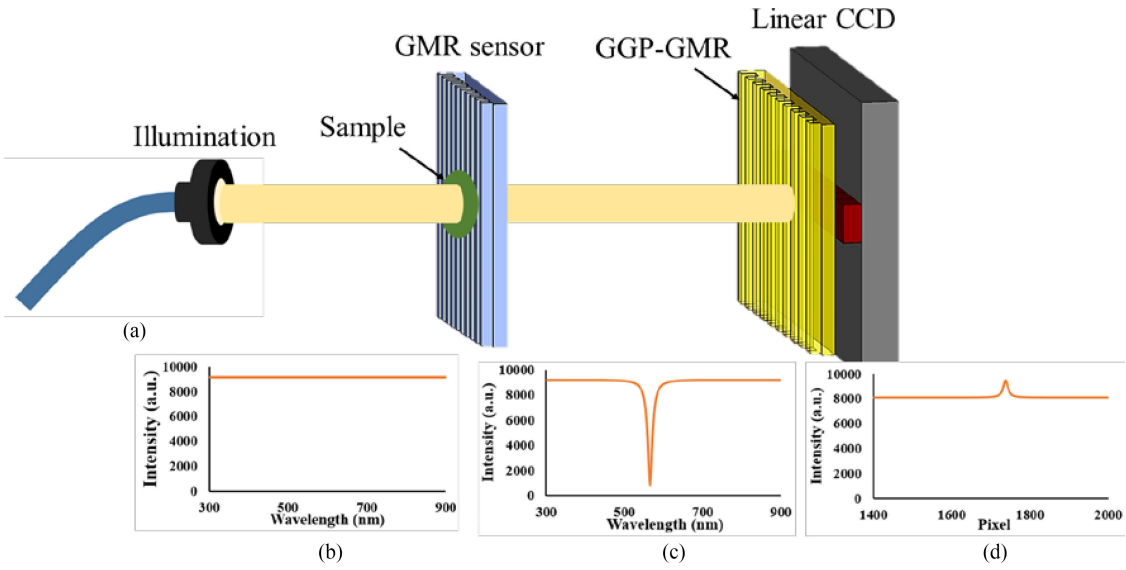


Fig. 4. (a) Schematic of the experimental setup. (a) Broadband illumination. (b) Dip transmission from the sensor response. (c) Peak response from the CCD measurement.

of light was reflected back; hence, a dip was measured within a transmission spectrum (Fig. 4(c)) as discussed in previous section. This spectrum was incident on a GGP-GMR and the transmitted intensity was measured by a linear CCD (Fig. 4(d)). The transmission peak at the CCD was correlated to the dip wavelength. Due to the nature of nonuniform broadband illumination and nonuniform transmission efficiency at different grating periods, the intensity measured at CCD was used as a reference for a broadband light source that was directly incident on the GGP-GMR without going through a GMR sensor. The transmission intensity distribution at CCD when the light went through the GMR sensor was then normalized to this reference signal such that a relative transmission spectrum as a function of the resonant pixel was obtained, whose peak was correlated to the dip wavelength. A brief and detailed discussion on the working principles can be found in supplementary materials and literature [21], respectively.

### *2.4 Experimental Verification on Dip Wavelength Monitoring*

To verify the proposed dip wavelength detection based on GGP-GMR and CCD system, two sets of experiments were performed: different GMR sensors with different resonant wavelengths and one GMR sensor with different sucrose solutions.

*2.4.1 GMR Sensors With Different Resonant Wavelengths:* A GMR sensor was used to verify the dip wavelength detection described in the previous section. A TM-polarized broadband light source (LS-1-LL, Ocean Optics) was deployed as shown in Fig. 5(a) and the transmission spectra (Fig. 5(b)) of the GMR were measured with a commercial spectrometer (USB2000+VIS-NIR-ES, Ocean Optics) indicating the resonant wavelength was 592 nm.

Two distributions of intensities were measured by the CCD when the broadband light source was incident on the GGP-GMR without and with going through the GMR sensor, which are indicated as broadband and sample in Fig. 5(c). By normalizing the CCD intensity measured from the sample to that of the broadband in Fig. 5(c), the relative transmission efficiency as a function of the pixel was obtained as shown in Fig. 5(d). The maximum transmission (approximately 89.7%) corresponded to pixel number 1120. Based on the resonant wavelength-pixel correlation (Fig. 3), that pixel corresponded to a wavelength of 592 nm, which was the dip wavelength measured by the Ocean Optics spectrometer (Fig. 5(b)). This example demonstrated that the dip wavelength

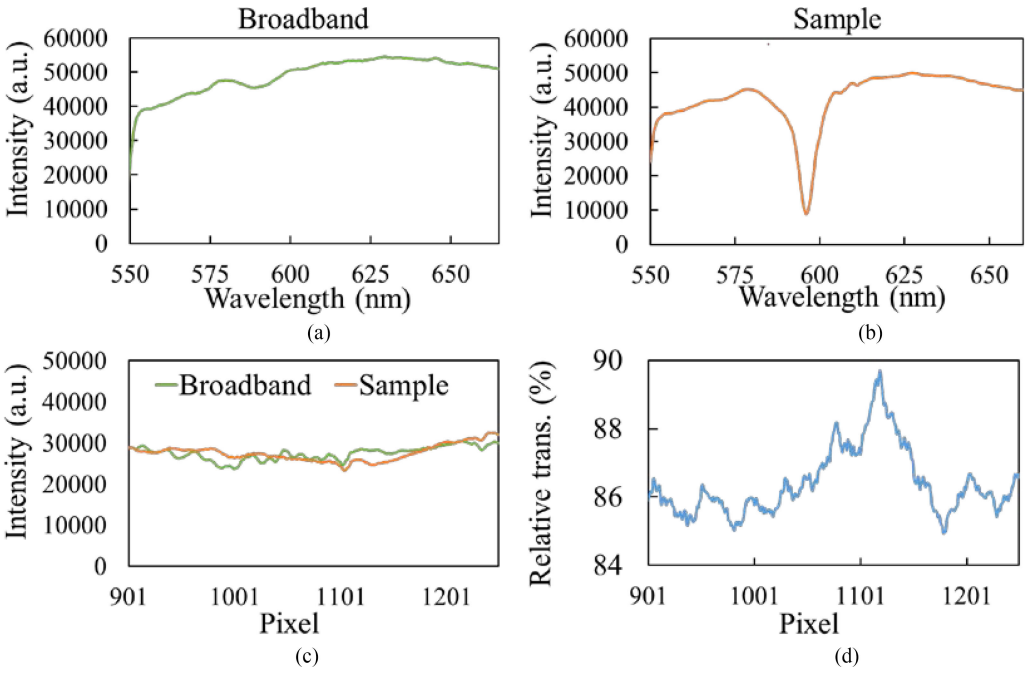


Fig. 5. Broadband light source (a) and transmission dip (b) measured with the Ocean Optics spectrometer. (c) Intensity distributions on the CCD for both broadband and sample illumination. (d) Relative transmission efficiency as a function of pixel obtained from (c).

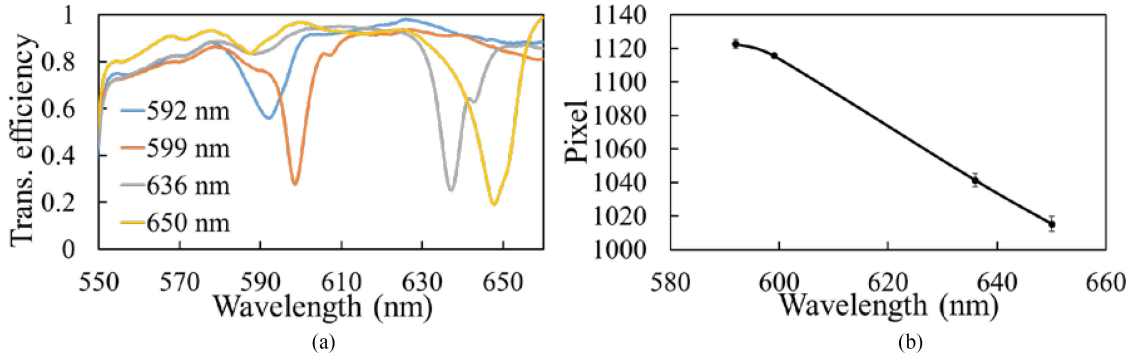


Fig. 6. (a) Normalized transmission spectra from four different GMR sensors. (b) Relationship between the relative peak transmission efficiency and the resonant wavelength of the GMR.

resulting from an optical sensor can be correlated to a resonant pixel in the GGP-GMR and CCD system based on a precalibrated wavelength–resonant pixel correlation (Fig. 3(d)).

To further solidify the concept, four GMRs with different resonant wavelengths (592, 599, 636, 650 nm) were tested (Fig. 6). The experiment started with the GMR at the lowest resonant wavelength and proceeded to the GMR at the highest resonant wavelength. For each GMR, the measurement process was the same as those described earlier such that for each GMR a corresponding pixel with highest relative transmission efficiency was obtained. Then the process was repeated another two times such that three measurements (relative maximum transmission efficiency) were taken for each GMR to minimize the experimental error, as summarized in Fig. 6(b). The results indicated that the pixel corresponding to the relative peak transmission efficiency indeed correlated well with the dip wavelength.

*2.4.2 GMR Sensor With Different Sucrose Concentrations:* For more practical applications or usage in biosensing, a resonant wavelength shift caused by the change of RI due to different

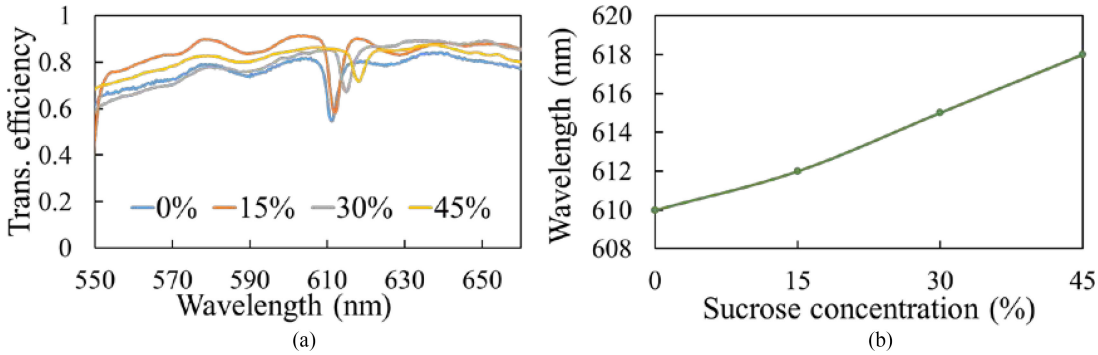


Fig. 7. (a) Transmission spectra of GMR sensor with various sucrose concentrations. (b) Relationship between dip wavelength and sucrose concentration.

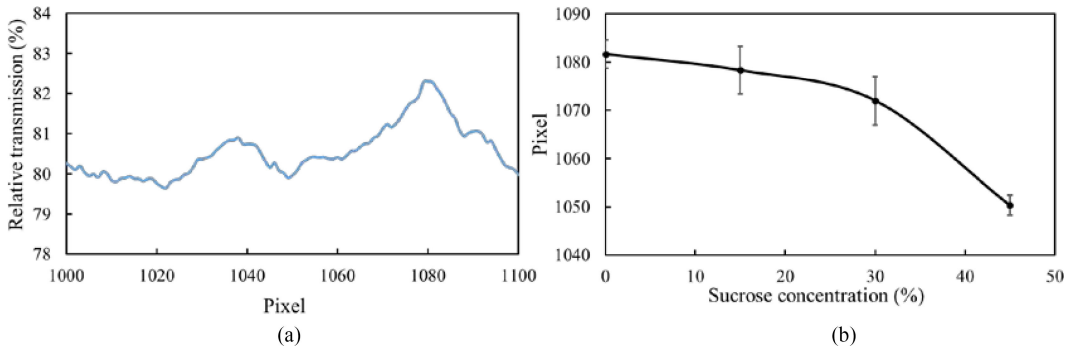


Fig. 8. (a) Relative transmission efficiency as a function of the pixel. (b) Relationship between the relative peak transmission efficiency corresponding pixel and sucrose concentration.

sample concentrations was used to test our GGP-GMR and CCD system. In this test, a GMR again was used as a biosensor, and sucrose samples with different concentrations were used as sample models. First, the Ocean Optics spectrometer was used to measure transmission spectra and dip wavelengths when samples were applied on the GMR sensor. The results indicated that the sucrose concentrations of 0, 15, 30 and 45% (the corresponding refractive indices, RIs, are 1.333, 1.356, 1.381, and 1.410 respectively) had resonant wavelengths at 611.30, 612.0, 615.10, and 618.21 nm respectively (Fig. 7).

For the GGP-GMR and CCD measurement, first, the transmitted intensity was recorded by the CCD when a broadband light source illuminated the GGP-GMR without going through a GMR sensor; that intensity was used as the reference signal. The CCD intensity for a droplet of sucrose applied on a GMR sensor was measured; it was then normalized to the reference signal to obtain the relative transmission efficiency as a function of the pixel. The experiment started with the lowest (0%, deionized water) concentration, and proceeded to the highest (45%) concentration. The GMR sensor was rinsed between each sample. The same procedure was repeated for another two runs such that for each concentration, three measurements were obtained.

Fig. 8 shows an example of relative transmission efficiency for 0% sucrose (water only). Peak finder from Origin Pro was used to better define the maximum transmission corresponding pixel, 1079, which corresponds to a wavelength of 612 nm based on the wavelength–resonant pixel correlation (Fig. 3(d)). This is close to but deviates slightly from the resonant wavelength (611.3 nm) measured by the Ocean Optics spectrometer. We discuss that deviation in a later section. Once again, this indicates that based on the maximum transmission corresponding pixel, one can determine the resonant wavelength. By monitoring the shift of the relative peak transmission corresponding pixel, one can determine the shift of the resonant wavelength. In turn, one can determine the

change of the RI; hence, one can determine the change of the sample concentration. The relative transmission peaks for four different sucrose concentrations are summarized in Fig. 8(b).

## 3. Discussion

In this work, we demonstrated a resonant wavelength detection system. The main difference between this work and our previous work [11], [12] are in two aspects. First, the system discussed in this work can only identify the dip wavelength (although theoretically the system can also detect the peak wavelength). However, our previous work with appropriate algorithms can reconstruct the whole spectrum. Second, practically, one can run the calibration curve to obtain the relationship between relative maximum transmission efficiency corresponding pixel and sample concentration as shown in Fig. 8(b) without any knowledge of Fig. 3(c). However such relationship between the pixel and the corresponding wavelength is required for our previous work to reconstruct the whole original spectrum.

To verify the proposed system, we demonstrated it can be used to track dip wavelengths resulting from different GMR sensors or the same GMR sensor covered with different sucrose solutions. It is to be understood that the purpose of a GMR sensor used in this work is only to generate a dip wavelength to verify the proposed concept. The GGP-GMR resonant wavelength detection system can be used with different sensors for various applications as long as the output having a dip wavelength or peak wavelength spectrum, such as surface plasmon resonance (SPR) [22] or localized SPR [23] biosensors, GMR strain sensors [24], or colloidal photonic crystal for fatigue monitoring [25]. To the best of our knowledge, the proposed system represents a novel resonant wavelength detection method. We believe there are plenty of room for improvement. In this section, we will discuss some potential improvement and other applications.

### *3.1 GGP-GMR System Performance*

From the Fig. 7, for the sucrose of 0% to 45%, the resonant wavelength shifted from 611.3 to 618.21 nm. Despite a slightly nonlinear response from Fig. 7(b), the bulk sensitivity defined as the change of wavelength to the change of RI was approximately 89.7 nm per refractive index unit (RIU). Based on the Section 2.2 and Fig. 3, the GGP-GMR has resolution of 1 nm; hence, for the GMR sensor used in this work, the smallest RIU can be measured was 0.011 RIU. However, it is to be understood that the GMR sensor used in this work is mainly for demonstration purposes — tracking the dip wavelength by the GGP-GMR and CCD system. To further optimize the GMR sensor, more thorough phenomenological analysis of waveguide grating coupling can be taken [26], [27]. If GMR or other type of biosensors with higher bulk sensitivity is used, the minimum detectable RIU can be further reduced.

### *3.2 High Q Resonance*

In this work, the GMR sensor was not optimized such that the coupling efficiency was not ideal as the transmission efficiencies were approximately 12% to 56% as shown in Fig. 6(a) and 55% to 72% as shown in Fig. 7(a). As suggested by Chang [21], a device with improved coupling efficiency (low transmission efficiency) would result in an improved signal. In this case, the difference between resonant (the relative peak transmission efficiency) to nonresonant pixel corresponding transmission efficiency (Fig. 4(c)) can be enhanced to minimize the measurement error, resulting in improved reliability.

### *3.3 Higher Wavelength Resolution*

The intrinsic limitation of the GGP-GMR used in this work can achieve 1-nm resolution, as shown in Fig. 3, where the minimum intensity corresponding pixels are at least 1 pixel apart for each 1-nm difference in incident wavelength. In turn, this limits the resolution of the measurements of

the sample concentrations. A sufficient difference in the sample concentration is required to cause a 1-nm wavelength shift from the biosensor. Several possible solutions might potentially improve the resolution. Currently, the GGP-GMR can only achieve a 2-nm increment on the grating period, which is limited by the available fabrication facility. Theoretically, if we can reduce the increment with better fabrication facility, the resolution can be further improved. Alternatively, a CCD with higher resolution (smaller pixel size) could improve the wavelength detection resolution even though that would reduce its sensitivity to light intensity. On the other hand, one can increase the repeated cycles for each period to increase the resolution with sacrifice of footprint of the GGP-GMR.

### *3.4 Peak Wavelength Detection*

In this paper, we only demonstrate that the GGP-GMR and CCD system can be used to monitor the dip wavelength by tracking the pixel corresponding to the relative peak transmission efficiency. However, based on a simulation [21], the system can be applied for tracking the shifts of the peak wavelengths in peak-type spectra. We are currently working on an experiment to verify the simulation result.

## 4. Conclusion

Currently, the spectrometer is one of the most commonly used pieces of equipment for tracking the peak or dip wavelengths in numerous biosensors and for determining the concentrations of relevant samples. It requires a certain optical path length for the required wavelength resolution, which makes it difficult to integrate with miniaturized sensor systems. In this work, we demonstrate that our GGP-GMR and CCD system can be used to monitor dip wavelengths. The demonstrated GGP-GMR is less than 1.8-mm long and yet the detection wavelength range can be 115 nm (550 to 665 nm) with a potential for 1-nm resolution. The device can be further optimized for even smaller size and higher resolution. With such a compact form factor, we believe it will have a great potential for integration with lab-on-a-chip systems or handheld devices for numerous sensing applications.

## Acknowledgment

The authors would like to thank the Nano Facility Center at National Chiao Tung University and National Nano Device Laboratories, Taiwan, for their support in fabricating and characterizing the GGP-GMR. We would also like to thank Wallace Academic Editing for editing this manuscript.

## References

[1] X. D. Fan, I. M. White, S. I. Shopova, H. Zhu, J. D. Suter, and Y. Sun, "Sensitive optical biosensors for unlabeled targets: A review," *Analytica Chimica Acta*, vol. 620, no. 1–2, pp. 8–26, Jul. 2008.
[2] J. Homola, "Present and future of surface plasmon resonance biosensors," *Anal. Bioanal. Chem.*, vol. 377, no. 3, pp. 528–539, Oct. 2003.
[3] Y. K. Tu, M. Z. Tsai, I. C. Lee, H. Y. Hsu, and C. S. Huang, "Integration of a guided-mode resonance filter with microposts for in-cell protein detection," *Analyst*, vol. 141, no. 13, pp. 4189–4195, 2016.
[4] B. Cunningham, P. Li, B. Lin, and J. Pepper, "Colorimetric resonant reflection as a direct biochemical assay technique," *Sensors Actuators B-Chem.*, vol. 81, no. 2–3, pp. 316–328, Jan. 2002.
[5] M. G. Scullion, A. Di Falco, and T. F. Krauss, "Slotted photonic crystal cavities with integrated microfluidics for biosensing applications," *Biosensors Bioelectron.*, vol. 27, no. 1, pp. 101–105, Sep. 2011.
[6] W. Liang, Y. Huang, Y. Xu, R. K. Lee, and A. Yariv, "Highly sensitive fiber Bragg grating refractive index sensors," *Appl. Phys. Lett.*, vol. 86, no. 15, Apr. 2005, Art. no. 151122.
[7] M. C. Oh, K. J. Kim, J. H. Lee, H. X. Chen, and K. N. Koh, "Polymeric waveguide biosensors with calixarene monolayer for detecting potassium ion concentration," *Appl. Phys. Lett.*, vol. 89, no. 25, Dec. 2006, Art. no. 251104.
[8] A. Szeghalmi, E. B. Kley, and M. Knez, "Theoretical and experimental analysis of the sensitivity of guided mode resonance sensors," *J. Phys. Chem. C*, vol. 114, no. 49, pp. 21150–21157, Dec. 2010.
[9] M. G. Scullion, T. F. Krauss, and A. Di Falco, "Slotted photonic crystal sensors," *Sensors*, vol. 13, no. 3, pp. 3675–3710, Mar. 2013.
[10] A. Emadi, H. Wu, G. D. Graaf, and R. Wolffenbuttel, "Design and implementation of a sub-nm resolution microspectrometer based on a linear-variable optical filter," *Opt. Exp.*, vol. 20, no. 1, pp. 489–507, Jan. 2012.

[11] H. A. Lin, H. Y. Hsu, C. W. Chang, and C. S. Huang, "Compact spectrometer system based on a gradient grating period guided-mode resonance filter," *Opt. Exp.*, vol. 24, no. 10, pp. 10972–10979, May 2016.
[12] H.-Y. Hsu, Y.-H. Lan, and C.-S. Huang, "A gradient grating period guided-mode resonance spectrometer," *IEEE Photon. J.*, vol. 10, no. 1, 2018, Art. no. 4500109.
[13] F. Meng *et al.*, "Waveguide-integrated photonic crystal spectrometer with camera readout," *Appl. Phys. Lett.*, vol. 105, no. 5, Aug. 2014, Art. no. 051103.
[14] J. Bao and M. G. Bawendi, "A colloidal quantum dot spectrometer," *Nature*, vol. 523, no. 7558, pp. 67–70, Jul. 2015.
[15] R. Magnusson and S. S. Wang, "New principle for optical filters," *Appl. Phys. Lett.*, vol. 61, no. 9, pp. 1022–1024, Aug. 1992.
[16] B. T. Cunningham, M. Zhang, Y. Zhuo, L. Kwon, and C. Race, "Recent advances in biosensing with photonic crystal surfaces: A review," *IEEE Sensors J.*, vol. 16, no. 10, pp. 3349–3366, May 2016.
[17] R. Magnusson *et al.*, "Photonic devices enabled by waveguide-mode resonance effects in periodically modulated films," *Proc. SPIE*, vol. 5225, pp. 20–34, 2003.
[18] H. A. Lin and C. S. Huang, "Linear variable filter based on a gradient grating period guided-mode resonance filter," *IEEE Photon. Technol. Lett.*, vol. 28, no. 9, pp. 1042–1045, May 2016.
[19] D. W. Dobbs, I. Gershkovich, and B. T. Cunningham, "Fabrication of a graded-wavelength guided-mode resonance filter photonic crystal," *Appl. Phys. Lett.*, vol. 89, no. 12, Sep. 2006, Art. no. 123113.
[20] P. C. Mathias, N. Ganesh, W. Zhang, and B. T. Cunningham, "Graded wavelength one-dimensional photonic crystal reveals spectral characteristics of enhanced fluorescence," *J. Appl. Phys.*, vol. 103, no. 9, May 2008.
[21] C.-W. Chang, "Development and applications of a detecting system based on gradient grating period guided-mode resonance," *M.S. thesis*, *Mech. Eng.*, National Chiao Tung Univ., Hsinchu, Taiwan, 2016.
[22] J. Lu *et al.*, "Immunoassay for detection of infliximab in whole blood using a fiber-optic surface plasmon resonance biosensor," *Anal. Chem.*, vol. 89, no. 6, pp. 3664–3671, Mar. 2017.
[23] L. Shang, C. Liu, B. Chen, and K. Hayashi, "Development of molecular imprinted sol-gel based LSPR sensor for detection of volatile cis-jasmone in plant," *Sensors Actuators B-Chem.*, vol. 260, pp. 617–626, May 2018.
[24] N. L. Privorotskaya, C. J. Choi, B. T. Cunningham, and W. P. King, "Sensing micrometer-scale deformations via stretching of a photonic crystal," *Sensors Actuators A-Physical*, vol. 161, no. 1–2, pp. 66–71, Jun. 2010.
[25] D. Zonta *et al.*, "Photonic crystals for monitoring fatigue phenomena in steel structures," *Proc. SPIE*, vol. 7292, 2009, Art. no. 729215.
[26] A. I. Avrutsky and V. A. Sychugov, "Reflection of a beam of finite size from a corrugated waveguide," *J. Modern Opt.*, vol. 36, no. 11, pp. 1527–1539, Nov. 1989.
[27] D. Pietroy, O. Parriaux, and J. L. Stehle, "Ellipsometric retrieval of the phenomenological parameters of a waveguide grating," *Opt. Exp.*, vol. 17, no. 20, pp. 18219–18228, Sep. 2009.